On the Structure of Trimethyltin Fluoride

Praveen Chaudhary,[a] Mario Bieringer,[b] Paul Hazendonk*[a] and Michael Gerken*[a]

a Department of Chemistry and Biochemistry and the
Canadian Centre for Research in Advanced Fluorine Technologies
University of Lethbridge, Lethbridge Alberta, T1K 3M4, Canada.
E-mail: michael.gerken@uleth.ca, paul.hazendonk@uleth.ca
b Department of Chemistry, University of Manitoba, 144 Dysart Road, Winnipeg, Manitoba, R3T2N2, Canada.

† Electronic supplementary information (ESI) available: ^{1}H MAS NMR spectra of non-recrystallized (Fig. S1) and recrystallized $(CH_3)_3SnF$ (Fig. S2), $^{13}C\{^{1}H,^{19}F\}$ MAS NMR spectrum of recrystallized $(CH_3)_3SnF$ (Fig. S3), experimental and simulated $^{19}F\{^{1}H\}$ MAS NMR spectra (Fig. S4 to S6), experimental and simulated $^{119}Sn\{^{19}F,^{1}H\}$ MAS NMR spectra (Fig S7) and $^{119}Sn\{^{1}H\}$ MAS NMR spectra (Fig. S8) of recrystallized $(CH_3)_3SnF$. CCDC 1400761 and 1400762.

Table of Content Entry

Contrary to previous reports, trimethyltin fluoride was shown to adopt a linear chain structure with symmetric fluorine bridges in the solid state.

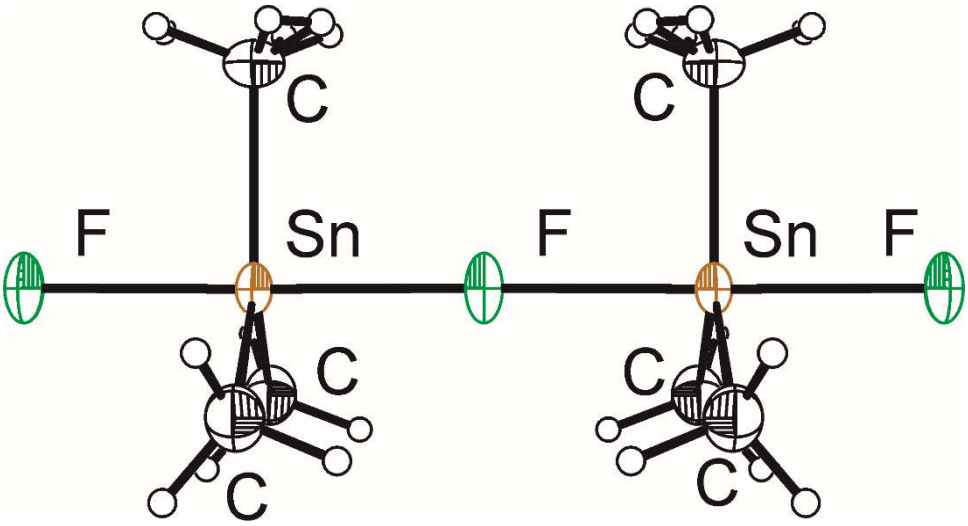

Abstract

The solid-state structure of $(CH_3)_3SnF$ was reinvestigated by X-ray diffraction techniques as well as multi-nuclear solid-state NMR spectroscopy. Trimethyltin fluoride crystallizes from hot ethanol in the orthorhombic space group *Pnma* at room temperature and changes to a low-temperature orthorhombic phase (space group: *Cmcm*) below −70 °C. In both modifications, trimethyltin fluoride adopts a linear chain structure with symmetric fluorine bridges, in contrast to previous reports. During its synthesis, $(CH_3)_3SnF$ precipitates in another, poorly crystalline modification, as shown by powder X-ray diffraction. Solid-state MAS NMR experiments of both room-temperature phases $(CH_3)_3SnF$ (non-recrystallized and recrystallized) were carried out for the ^{1}H, ^{13}C, ^{19}F, and ^{119}Sn nuclei. The $^{119}Sn\{^{19}F, ^{1}H\}$ and $^{19}F\{^{1}H\}$ NMR spectra offer unambiguous determination of the ^{19}F and ^{119}Sn shielding tensors. The $^{119}Sn\{^{1}H\}$ solid-state NMR spectra agree with pentacoordination about Sn in this compound for the non-recrystallized and the recrystallized modifications. Based on the solid-state NMR results, the non-crystallized modification of $(CH_3)_3SnF$ also consists of linear, symmetrically fluorine-bridged chains, and differs from the recrystallized orthorhombic phases only in packing of the chains.

Introduction

Trimethyltin fluoride is the simplest member of the group of triorganyltin fluoride. It has attracted interest in organometallic chemistry as a fluorinating agent of group 4 to 6 compounds and some main-group chlorides,[1] and is readily prepared by halogen exchange from $(CH_3)_3SnCl$ and KF in a water-ethanol mixture.[2] Trimethyltin fluoride is insoluble in most organic solvents except in hot alcohols and melts upon decomposition at a relatively high temperature (375 °C), which is strongly indicative of its aggregation in the solid state. Trimethyltin fluoride was the first triorganotin fluoride to be studied by X-ray crystallography;[3] however, the structural characterization proved to be problematic. Clark *et al.* reported that disorder precluded the proper refinement of its structure.[3] Two possible disorder models were put forward, both invoking fluorine-bridged chain motifs. The first model proposes a pyramidalized trimethylstannyl moiety with disordered fluorine atoms and bent Sn–F---Sn bridges. The chains, and hence, the orientation of the pyramidalized trimethylstannyl moieties can be randomly oriented along the chain axis. The second model invokes planar trimethylstannyl groups that are tilted in alternating fashion along the chain axis. The disordered fluorine atoms form bent Sn–F---Sn bridges while the F–Sn---F units are linear. The observation of one SnC_3 stretching band in the infrared spectrum (550 cm^{-1}, ν_{as}) and two SnC_3 stretching bands in the Raman spectrum (517 cm^{-1}, ν_s and 556 cm^{-1}, ν_{as}) was found to be more congruent with a planar SnC_3 arrangement, providing evidence against the first disorder model.[4] The second disorder model was also rejected model upon careful reevaluation of the single crystal X-ray diffraction data which did not exhibit diffraction spots indicative of doubling in one cell axis, which is to be expected in case of alternate tilting in successive $Sn(CH_3)_3$ groups.[4] Hence, it was necessary to propose a new model with parallel planar SnC_3 moieties and

positional disorder in the fluorine atoms with asymmetric fluorine bridges (Sn–F: 2.15 Å, Sn---F: 2.45 Å) and Sn–F---Sn and F–Sn---F angles of 141°.

Crystallographic studies show that monomeric R_3SnF adopt tetracoordinate tin configurations when the R groups have sufficient steric bulk. Examples for this structural motif are seen for trimesityltin fluoride, Mes_3SnF (Mes = mesityl),[5] $(PhMe_2Si)_3CSnMe_2F$,[6] and $(Me_3Si)_3CSnPh_2F$.[6] For less bulky substituents fluorine is able to serve as a bridging atom, resulting in chain structures composed of penta-coordinate tin centres. Chain structures of this kind were observed for Ph_3SnF,[7] $(PhCH_2)_3SnF$, [8] $(Me_3SiCH_2)_3SnF$, [9] and tricyclohexyltin fluoride; [10] however one should note that problems were encountered with three of these structure. The structure of $(PhCH_2)_3SnF$ was only reported in a Ph.D. thesis, exhibiting very large uncertainties in the Sn–F distances. Whereas tricyclohexyltin fluoride had previously been incorrectly reported to be monomeric with tetracoordinate tin centres,[11] a disorder in the structure of $(Me_3SiCH_2)_3SnF$ was overlooked in the original paper.[12]

Multi-nuclear solid-state NMR spectroscopy is very useful in obtaining structural information of triorganyltin fluorides as ^{119}Sn and ^{19}F are NMR-active relatively abundant spin-½ nuclei. Monomeric structures with tetracoordinate tin, such as Mes_3SnF, exhibit a doublet splitting in the ^{119}Sn MAS NMR spectrum due to $^{1}J(^{119}Sn\text{-}^{19}F)$ coupling with an associated coupling constant around 2300 Hz.[13] It is noteworthy that two doublets were observed for Mes_3SnF because of the two crystallographically independent Mes_3SnF molecules in the unit cell. Triplet splitting patterns are typical in the ^{119}Sn MAS NMR spectra of fluorine-bridged chain compounds owing to the indirect coupling to two fluorine environments. For example, the ^{119}Sn MAS NMR spectrum of tris(iso-butyl)tin fluoride shows a spinning sideband manifold composed of triplets with a $^{1}J(^{119}Sn\text{-}^{19}F)$ coupling constant of 1260 Hz.[14]

Harris *et al.* have studied $(CH_3)_3SnF$ among other triorganotin fluorides by MAS NMR spectroscopy.[13,15] A sideband manifold of triplets (δ_{iso}= 24.3 ppm) was observed in the $^{119}Sn\{^1H\}$ MAS NMR spectrum of $(CH_3)_3SnF$ with a $^1J(^{119}Sn\text{-}^{19}F)$ constant of 1300 Hz. Analysis of the sideband pattern yielded a chemical shift anisotropy of −221 ppm along with an asymmetry factor of 0 for the ^{119}Sn shielding tensor. Axial symmetry in this tensor was assumed in their analysis, although it seems to be at odds with the reported crystal structure.

The controversial nature of the reported crystal structure of $(CH_3)_3SnF$, as well as the apparent disagreement between the structure and the solid-state NMR spectroscopic data prompted us to reevaluate the structure of this important tin halide and to determine whether the data from both techniques could ultimately be reconciled.

Results and Discussion

X-Ray Diffraction.

Crystals of $(CH_3)_3SnF$ were grown from hot ethanol as bundles of very fine needles. These crystals are extremely fragile, as needles that initially looked single under the microscope fell apart into thinner needles upon manipulation. Consequently they were very difficult to mount as single crystals without cleaving them into smaller needles, which is consistent with their weak interchain interactions previously noted.[3] In most cases the diffraction spots of what appeared to be a single needle were elongated, suggesting that the packing of the chains was disordered to some degree. The indexing of the room-temperature single-crystal data always produced the same orthorhombic unit cell as previously reported.[3] The refinement using the initially collected data showed similar problems encountered by Clark *et al.*, that, for example, the electron density on two carbon atoms is smaller than that on the remaining carbon. Attempts to anisotropically refine all non-hydrogen

atoms were unsuccessful. Ultimately, after growing and screening many crystals, one specimen was found that gave diffraction spots with minimal elongation. The room-temperature, as well as low-temperature (−120 °C), data of this crystal were obtained, giving structures that could be anisotropically refined. Selected crystallographic data are listed in Table 1, while the most important bond lengths and angles are listed in Table 2.

Table 1 Crystallographic Data for $(CH_3)_3SnF$.

Chem formula	$(CH_3)_3SnF$	$(CH_3)_3SnF$
Mass [g mol^{-1}]	182.79	182.79
Crystal system	Orthorhombic	Orthorhombic
Space group	*Pnma*	*Cmcm*
a [Å]	12.831(4)	4.3304(4)
b [Å]	4.3239(13)	12.6670(13)
c [Å]	10.846(3)	10.5740(11)
V [Å^3]	601.7(3)	580.02(10)
Z	4	4
Calcd density [g cm^{-3}]	2.018	2.093
T [°C]	23	−120
μ [mm^{-1}]	4.123	4.277
R_1[a]	0.0423	0.0206
wR_2[b]	0.1130	0.0590

[a] R_1 is defined as $\Sigma||F_o| - |F_c||/\Sigma|F_o|$ for $I > 2\sigma(I)$. [b] wR_2 is defined as $[\Sigma[w(F_o^2 - F_c^2)^2]/\Sigma w(F_o^2)^2]^{1/2}$ for $I > 2\sigma(I)$.

Table 2 Selected bond lengths [Å] and angles [deg.] for the 23 and −120 °C crystal structures of $(CH_3)_3SnF$.

Pnma (23 °C)			
Sn−F	2.1620(7)	Sn−F−Sn	179.2(3)
		F−Sn−F	179.2(3)
Sn−C	2.122(13)	C−Sn−C	119.0(5)
	2.105(11)		121.2(5)
	2.106(10)		119.8(5)
Cmcm (−120 °C)			
Sn−F	2.1652(2)	Sn−F−Sn	179.5(2)
		F−Sn−F	179.5(2)
Sn−C	2.120(5)	C−Sn−C	121.07(15)
	2.120(5)		121.07(15)
	2.113(7)		117.9(3)

At room temperature trimethyltin fluoride crystallizes in the orthorhombic space group *Pnma* in agreement with Clark *et al.*[3] In contrast to the previously reported structure, the structure reported herein was anisotropically refined as a linear chain with symmetric fluorine bridges, likely because of the superior quality of the current crystal. Attempts to refine two fluorine positions as a disordered asymmetric bridge failed and no evidence for tilting of the trimethyltin moiety along the chain was found. The trimethyltin moiety was found to be trigonal planar. The fluorine bridge is symmetric with an Sn−F distance of 2.1620(7) Å and essentially linear. At −120 °C, $(CH_3)_3SnF$ crystallizes in an orthorhombic unit cell of similar cell lengths; the space group; however, changes to *Cmcm*. The geometry of the $(CH_3)_3SnF$ chains does not change appreciably during the phase transition, retaining the linear symmetric fluorine bridge in the structure (Fig. 1). The Sn−F distance of 2.1652(2) Å (−120 °C) compares well with the Sn−F distance reported for the linear symmetrically bridge chain structure of Ph_3SnF (2.1458(3) Å),[7] being the only other structurally characterized triorganotin fluoride with a linear symmetrically bridged chain structure. The phase transition is accompanied by a change in packing of the linear chains (Fig. 2). In both structures,

the chains are aligned with the shortest cell axis (*b*-axis in the *Pnma* structure, *a*-axis in the *Cmcm* structure). No significant interchain interactions are present in both structures, which accounts for the fragility of the macroscopic needle-shaped crystals. Whereas the packing of the chains along the *c*-axis (10.846(3) Å for the *Pnma* structure; 10.5140(11) Å for the *Cmcm* structure) is the same, the adjacent layers of $(CH_3)_3SnF$ chains are shifted upon phase transition. As the covalently bonded environment does not change between 23 and −120 °C, no differences were observed in Raman spectra upon lowering the temperature.

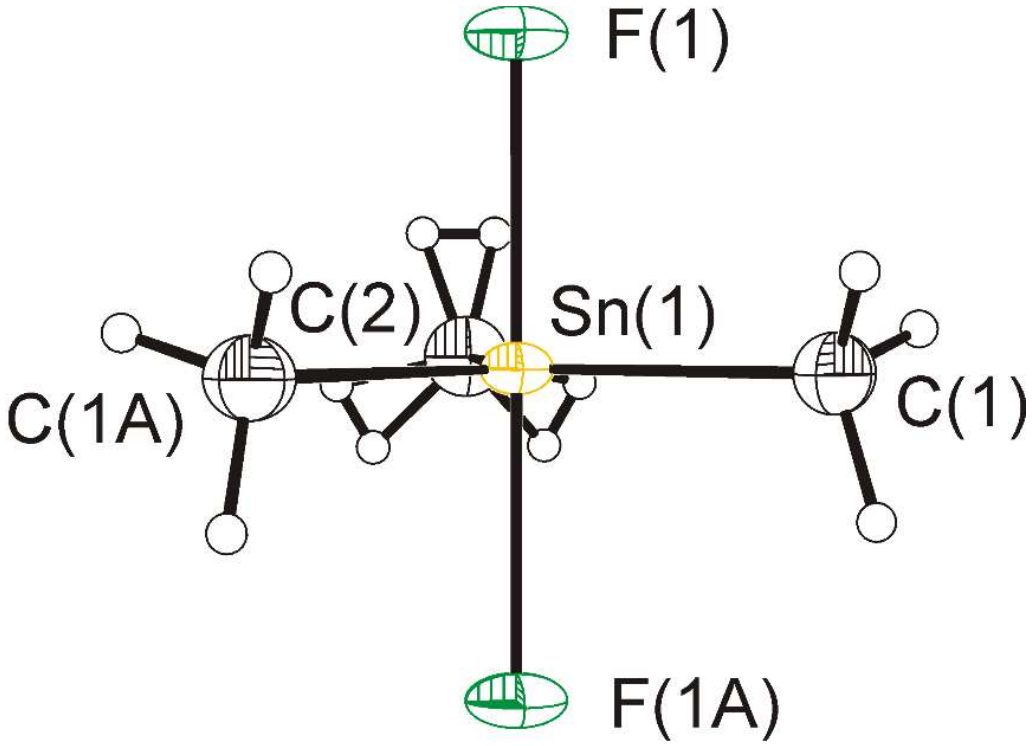

Fig. 1 Thermal ellipsoid plot of the $FSn(CH_3)_3F$ moiety in the −120 °C crystal structure of $(CH_3)_3SnF$. Thermal ellipsoids are drawn at the 50% probability level.

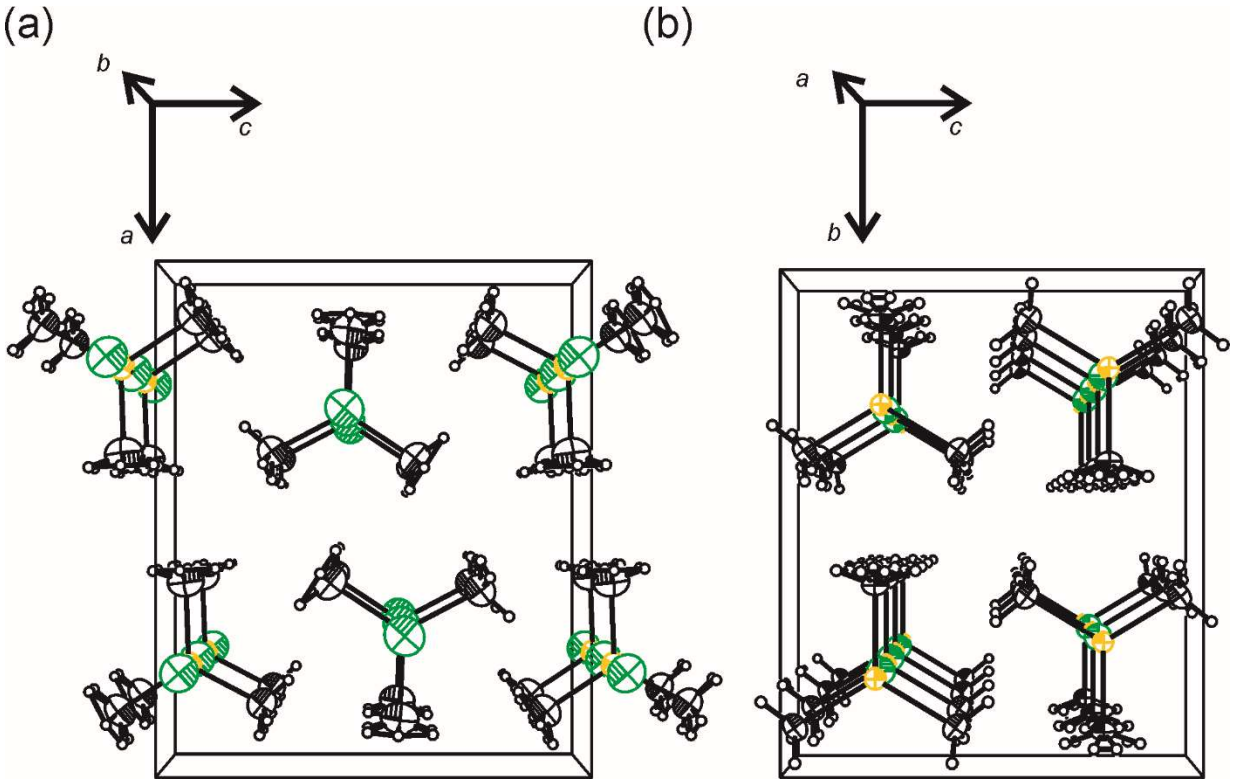

Fig. 2 Views of the packing of the chains in $(CH_3)_3SnF$ (a) along the *b*-axis (23 °C) and (b) along the *a*-axis (−120 °C). Thermal ellipsoids are drawn at the 50% probability level.

In order to ascertain the purity of the bulk sample, a room-temperature powder X-ray diffraction pattern was acquired of non-recrystallized $(CH_3)_3SnF$. Surprisingly, this diffraction pattern contained broad powder diffraction peaks that were not indexable on the *Pnma* and *Cmcm* structures, indicating a different, poorly crystalline phase. In contrast, a ground recrystallized sample was highly crystalline and its powder diffraction pattern agreed with the *Pnma* structure. The poorly crystalline phase, however, was still present as a minor phase in the recrystallized sample. Fig. 3 shows the LeBail fit in space group *Pnma* with very reasonable agreement, differences between the diffraction data and the *Pnma* model can be attributed to the impurity phase. The unit cell dimensions for the crystalline phase obtained from the LeBail fit (a = 12.831(2) Å, b = 4.319(2) Å and c = 10.839(2) Å) are in excellent agreement with those obtained by the

single-crystal analysis. It is not possible to quantify the phase ratio in the recrystallized sample from the powder diffraction data, but it is obvious that the poorly crystalline phase is a minor phase likely less than 20% by mass, which is in agreement with the ^{13}C NMR data (vide infra). It is proposed that the non-recrystallized phase is a kinetic product obtained by precipitation from a water-ethanol mixture at room temperature, whereas the re-crystallization from hot ethanol results in the thermodynamically preferred *Pnma* structure. The fragile nature of the $(CH_3)_3SnF$ needles suggest that rapid crystallization will result in smaller crystalline domain sizes. The symmetric line shape of the broad peaks in the powder X-ray pattern of the non-recrystallized sample is in agreement with the crystalline domains being small in all three dimensions. Notably the *Pnma* structure is not detectable in the non-recrystallized sample.

Variable-temperature powder X-ray diffraction of the recrystallized phase showed the phase transition between the *Pnma* and *Cmcm* modifications occurring at −70 °C. No change of the X-ray powder pattern of the non-recrystallized sample was observed in the temperature range from 20 to −120 °C. It is noteworthy that the Raman spectra of the three modifications, i.e., non-recrystallized and the two recrystallized modifications, and the infrared spectra of the two room-temperature modifications were essentially identical, suggesting the same local geometries within all modifications.

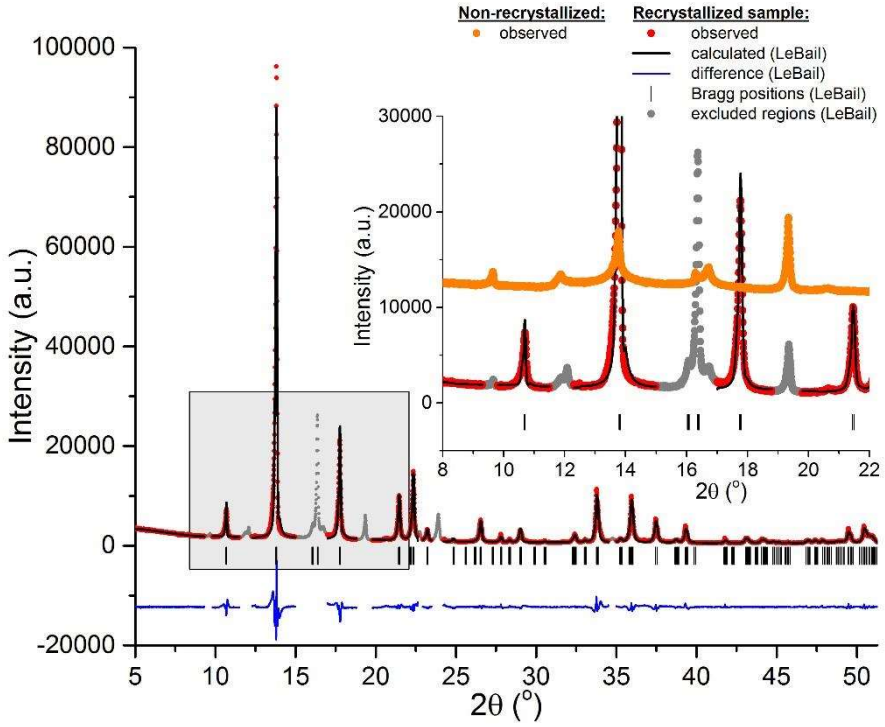

Fig. 3 Powder X-ray diffraction patterns of recrystallized $(CH_3)_3SnF$ (red trace), non-recrystallized $(CH_3)_3SnF$ (orange trace in insert). The grey sections indicate the regions that were excluded from the refinement.

Solid-State NMR Spectroscopy.

Non-recrystallized as well as recrystallized $(CH_3)_3SnF$ were studied by multi-nuclear solid-state NMR spectroscopy at 20 °C. The solid-state NMR studies in the literature[13,15,16] have presumably been carried out on the non-recrystallized modification, since the existence of a separate modification was not known at that point of time.

The $^1H\{^{19}F\}$ MAS NMR spectra of $(CH_3)_3SnF$ were recorded at 20 °C (Fig. S1 and S2, ESI†) showing one ^1H resonance at 0.63 ppm (non-recrystallized sample) and 0.51 ppm (recrystallized sample) attributable to the methyl protons, in addition to background signals at 6.91

or 8.00 ppm arising from the Vespel™ or Torlon™ polymer materials, respectively, used for the low-fluorine-background end cap and drive tip of the rotor. A ^{19}F-to-^{1}H cross polarization NMR experiment (Fig. S1, ESI†) resulted in the sole observation of the methyl ^{1}H NMR signal of $(CH_3)_3SnF$. Typically ^{1}H NMR spectra are severely broadened by the strong homonuclear dipolar coupling. In contrast, the methyl signals in the ^{1}H NMR spectra are atypically narrow with half-widths, $\Delta\nu_{1/2}$, of 1340 (non-recrystallized) and 1450 Hz (recrystallized). This relatively good resolution is presumably a consequence of very rapid rotation about the Sn–C bond, scaling the dipolar coupling amongst the protons (typically 15 to 20 kHz) to a much reduced value (*ca.* < 1 kHz, the motionally averaged homonuclear dipolar and shielding tensors become orientationally coincident). This is further supported by the significantly reduced range and intensities of the sidebands.

Simultaneously decoupled ^{13}C{^{1}H,^{19}F} MAS NMR spectra of $(CH_3)_3SnF$ at spinning rates of 21 kHz revealed only a single resonance for the non-recrystallized sample ($\Delta\nu_{1/2}$ = 80 Hz) (Fig. 4) with an isotropic chemical shift of 2.3 ppm. Satellites result from coupling to the ^{117,119}Sn nuclei with $^{1}J(^{117,119}\text{Sn-}^{13}\text{C})$ = 511 Hz. Because the ratio of the magnetogyric ratios of ^{119}Sn to that of ^{117}Sn is 1.046, the satellites arising from coupling to the two nuclei could not be resolved. The sole CH_3 signal indicates the equivalence of all the methyl groups on the NMR time scale, which along with the lack of spinning sidebands implies rapid interchange between the three methyl groups about the tin at ambient temperature via rapid rotation of the chains along the chain axis in the solid state.

Lockhart and Manders[16] had reported the ^{13}C{^{1}H} MAS NMR spectrum of $(CH_3)_3SnF$ and a $^{1}J(^{119}\text{Sn-}^{13}\text{C})$ coupling of 550 Hz, which, however, was not well resolved due to coupling to ^{19}F, rendering the coupling constant from the double-decoupled spectrum to be a more reliable value.

Based on the structural analysis of methyltin polymers using ^{13}C solid-state NMR spectroscopy Lockhart and Manders proposed an empirical relationship between $^{1}J(^{119}Sn\text{-}^{13}C)$ and Me–Sn–Me bond angle (θ) for a variety of organotin polymers (eqn (1)).[16,17]

$$|^{1}J(^{119}Sn\text{-}^{13}C)| = (10.7 \pm 0.5)(\theta) - (778 \pm 64) \quad (1)$$

The Me–Sn–Me angle calculated using $^{1}J(^{117,119}Sn\text{-}^{13}C) = 511$ Hz is 120 ± 8°, suggesting the trigonal planar arrangement of the trimethylstannyl group. The $^{13}C\{^{1}H,^{19}F\}$ MAS NMR spectrum of recrystallized $(CH_3)_3SnF$ contained a singlet at 2.8 ppm with $^{117,119}Sn$ satellites (Fig. S3, ESI†). The $^{1}J(^{117,119}Sn\text{-}^{13}C)$ coupling constant of 520 Hz, which was obtained by deconvolution, corresponds to a Me–Sn–Me angle of 121 ± 8°, agreeing with the planar trimethylstannyl moiety observed in the crystal structure. The slight difference in ^{13}C chemical shifts between the two modifications of $(CH_3)_3SnF$ enabled the observation of the poorly crystalline phase impurity in the recrystallized sample as a shoulder, which represents approximately 15% as estimated by deconvolution (Fig. S2, ESI†).

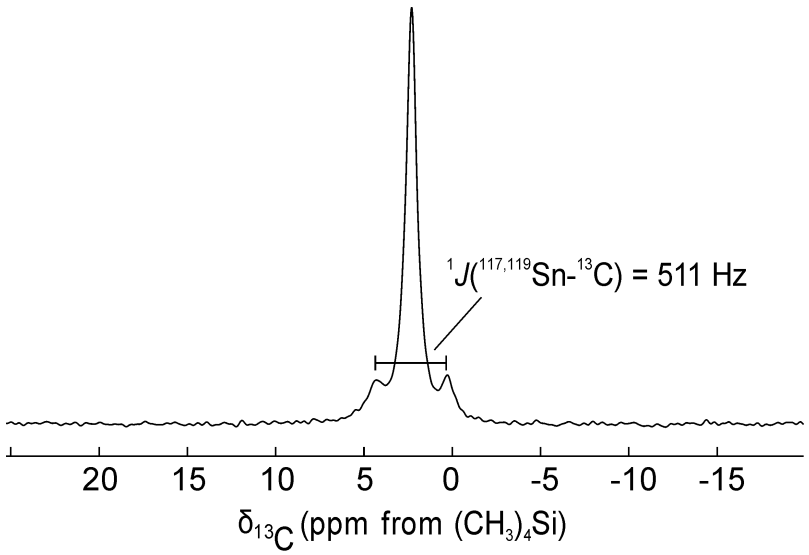

Fig. 4 Solid-state $^{13}C\{^{1}H,^{19}F\}$ MAS NMR spectrum of non-recrystallized $(CH_3)_3SnF$ at a spinning rate of 21 kHz at 20 °C.

The $^{19}F\{^{1}H\}$ MAS NMR spectrum recorded of non-recrystallized $(CH_3)_3SnF$ with a spinning rate of 24 kHz shows a spinning sideband manifold centered around a singlet at −134.9 ppm ($\Delta\nu_{1/2}$ = 350 Hz) with doublet satellites corresponding to $^{1}J(^{117/119}Sn\text{-}^{19}F)$ = 1230 Hz (Fig. 5). Because of sufficient signal-to-noise ratio and resolution, it was possible to observe the low-intensity two outer transitions of the triplet subspectrum arising from coupling of ^{19}F to two $^{117/119}Sn$ (Fig. S4, ESI†), evidencing the fluorine-bridged chain nature of $(CH_3)_3SnF$ in this poorly crystalline phase. The combination of decoupling and spinning at 24 kHz reduced both the homonuclear and heteronuclear dipolar couplings, and thus these couplings are not expected to significantly affect the sideband intensities, thereby allowing the ^{19}F chemical shielding tensor parameters to be obtained in isolation to high accuracy. Spectral simulation yielded an axially symmetric shielding tensor, i.e., asymmetry parameter $\eta = 0$, with an anisotropy of 55.4 ± 0.4 ppm (Fig. S5, ESI†).

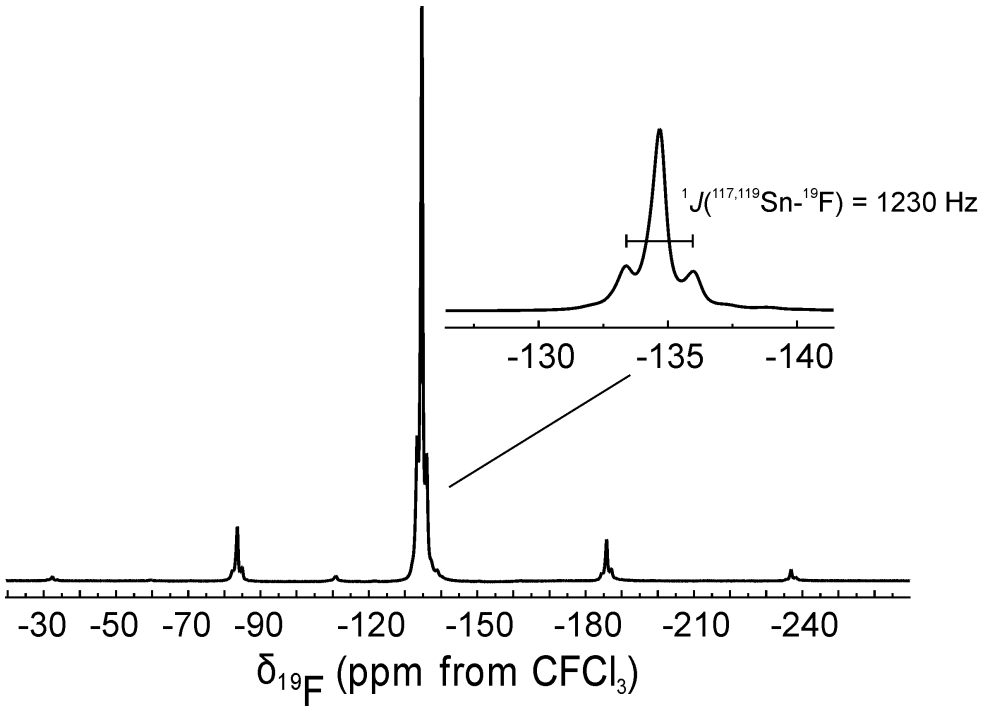

Fig. 5 Solid-state $^{19}F\{^{1}H\}$ MAS NMR spectrum of non-recrystallized $(CH_3)_3SnF$ at a spinning rate of 24 kHz, at 20 °C.

The $^{119}Sn\{^{1}H,^{19}F\}$ MAS NMR spectra (Fig. 5) show the spinning side-band manifold of a singlet (δ_{iso} = 24.3 ppm). Spectral simulation gave a shielding anisotropy of −235 ± 5 ppm and an asymmetry parameter of 0. The shielding anisotropy obtained from the simultaneously-decoupled spectra is in the same order of magnitude as that previously reported by Harris (−221 ppm).[15] The axially symmetry of the ^{19}F and ^{119}Sn shielding tensors suggests the linear environments about F and Sn in the chain structure for non-recrystallized $(CH_3)_3SnF$.

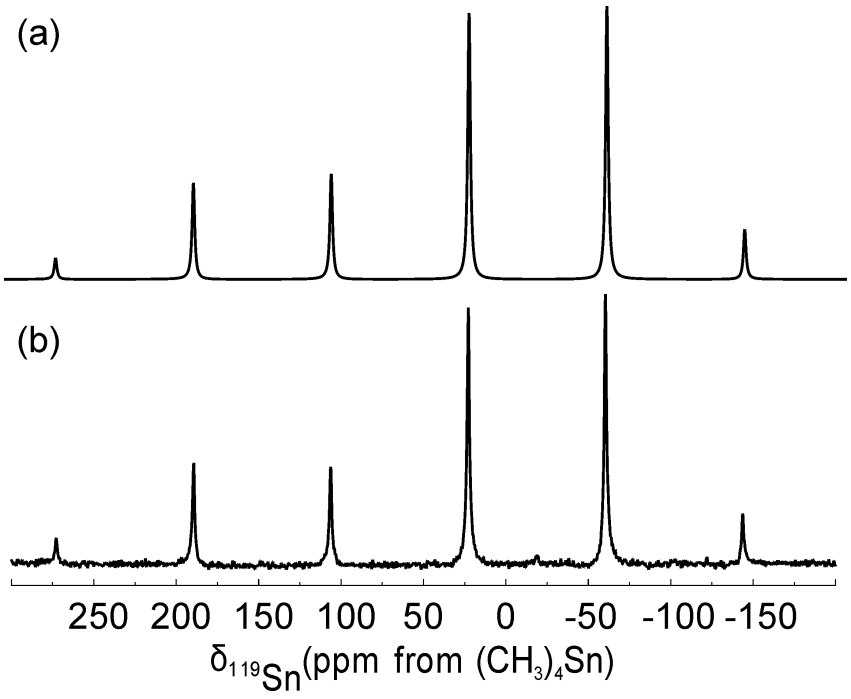

Fig. 6 (a) Simulated and (b) experimental solid-state $^{119}Sn\{^{1}H,^{19}F\}$ MAS NMR spectrum of non-recrystallized $(CH_3)_3SnF$ at a spinning rate of 15.5 kHz at 20 °C.

High-resolution $^{119}Sn\{^{1}H\}$ MAS NMR spectra consist of spinning sideband manifolds of triplets centred at δ_{iso} = 23.2 ppm with $^{1}J(^{119}Sn\text{-}^{19}F)$ = 1280 Hz (Fig. 7), which is in good agreement with the values obtained by Harris.[13] The shielding tensor parameters for the ^{119}Sn and ^{19}F nuclei

obtained from the double-decoupled and ^{1}H-decoupled spectra, respectively, are now employed in the simulation of the ^{119}Sn{^{1}H} spectra to determine the remaining dipolar coupling parameters.

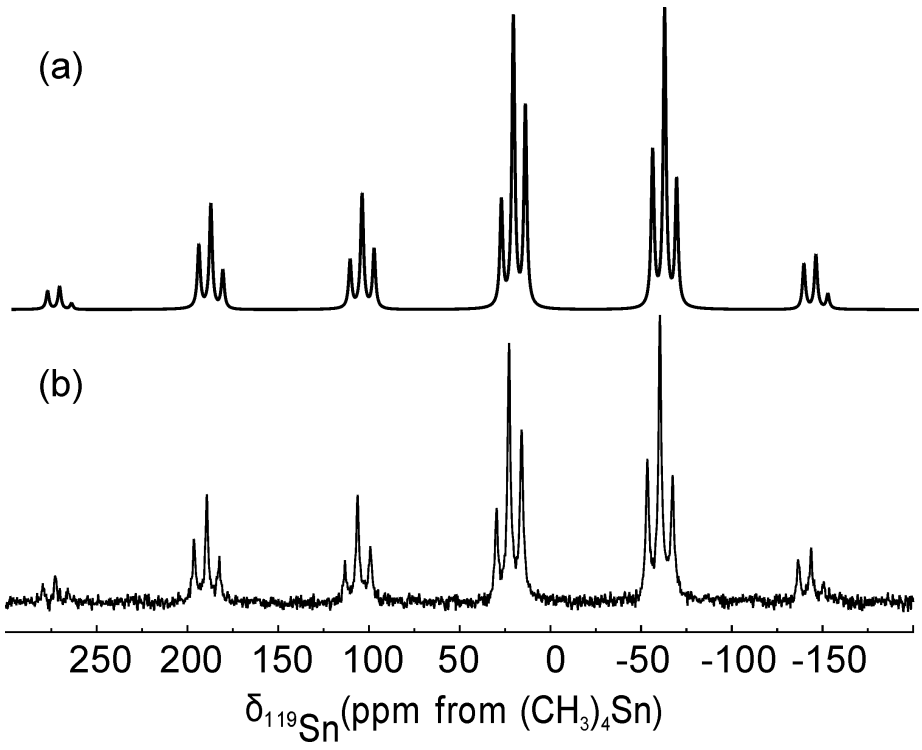

Fig. 7 (a) Simulated and (b) experimental solid-state ^{119}Sn{^{1}H} MAS NMR spectrum of non-recrystallized $(CH_3)_3SnF$ at a spinning rate of 15.5 kHz at 20 °C.

Notably, the triplets in the ^{119}Sn{^{1}H} MAS NMR spectra arising from *J*-coupling to two equivalent fluorines exhibit a roofing effect due to residual effects from the anisotropy in the indirect coupling tensor, ΔJ, and dipolar coupling that is still present at this spinning rate. Simulation yields an effective dipolar coupling constant D', which is related to the dipolar coupling constant D and ΔJ by eqn (2):

$$D' = D - \frac{\Delta J}{3} \qquad (2)$$

The dipolar coupling constant D was calculated assuming the same Sn−F distance that was obtained by X-ray crystallography for the crystalline *Pnma* modification using eqn (3) as 4200 Hz.

$$D = \frac{\mu_0}{4\pi}\frac{\gamma_A\gamma_X}{r_{AX}^3} \quad (3)$$

In this manner ΔJ can be determined to be −500 ± 200 Hz, which represents one of the few experimentally determined ΔJ values.

The $^{19}F\{^1H\}$ MAS NMR spectrum (Fig. S6, ESI†) of recrystallized $(CH_3)_3SnF$ shows a spinning side band manifold of singlets with ^{119}Sn satellites with the same isotropic chemical shift (δ_{iso} = −134.3 ppm) and $^1J(^{117,119}Sn\text{-}^{19}F)$ coupling constant (1230 Hz) as the other room-temperature phase of $(CH_3)_3SnF$. As expected from the presence of the ca. 15% of phase impurity, the relative intensities of the spinning sidebands could not be simulated using a single tensor. Including 15% of a component with δ_{aniso} = 55.4 ppm and η = 0, gave an axial symmetric shielding tensor for the orthorhombic crystalline phase (85%) with an anisotropy of approximately 51 ppm. Likewise, the spinning sideband manifold around the isotropic signal (δ_{iso} = 22.9 ppm) in the $^{119}Sn\{^{19}F,^1H\}$ NMR spectra of recrystallized $(CH_3)_3SnF$ could not be simulated with a single tensor. Even when considering the 15% phase impurity (δ_{aniso} = −235 ppm and η = 0), at least two more axially symmetric tensors had to be included in the simulations to give a satisfactory fit of the spinning sideband manifolds (57%: δ_{aniso} = −204 ppm and η = 0; 28%: δ_{aniso} = −295 ppm and η = 0) (Fig. S7, ESI†). The consideration of non-axially symmetric shielding tensors did not produce good agreements between the simulated and experimental spectra. Based on the powder X-ray diffraction results, the correlation of the two additional tensor components to separate phases is excluded. While the origin of the necessity to use at least two tensors in addition to that of the known phase impurity is not understood, it could be a consequence of sensitivity of the ^{119}Sn tensor to small changes in Sn−F bond lengths, possibly through vibrations. As for the ^{19}F, the ^{119}Sn

shielding tensor was found to be axially symmetric, agreeing with the fluorine-bridged linear chain structure observed in the crystal structure of recrystallized $(CH_3)_3SnF$. The anisotropy in $^1J(^{119}Sn-^{19}F)$, ΔJ, determined from the slanting of the outer transitions of the triplet in the ^1H-decoupled ^{119}Sn NMR spectrum (Fig. S8, ESI†), is indistinguishable from that obtained for the non-recrystallized sample (approximately −500 Hz).

Conclusion

After controversy about the solid-state structure of trimethyltin fluoride, which is the parent triorganotin fluoride compound and has importance as a reagent in inorganic chemistry, it was shown to adopt a linear chain structure with symmetric fluorine bridging. The current study corrects the previous report, which has puzzled chemists because of its non-intuitive structural description, as well as an apparent conflict with solid-state NMR spectroscopic data. Conclusive high-resolution solid-state NMR spectroscopic data of $(CH_3)_3SnF$ were obtained using fast spinning along the magic angle as well as double decoupling techniques. In addition to two crystalline phases (space groups *Pnma* (20 °C) and *Cmcm* (−120 °C)) a poorly crystalline phase was identified that is formed when synthesizing $(CH_3)_3SnF$ from a water-ethanol mixture at room temperature. The similarity of isotropic chemical shifts and the axial symmetric nature of the ^{19}F and ^{119}Sn shielding tensors in recrystallized and non-recrystallized $(CH_3)_3SnF$ provide strong evidence for the same linear chain structure of all currently identified phases of $(CH_3)_3SnF$. The most significantly different isotropic chemical shift between the poorly crystalline and crystallized phases was $\delta_{iso}(^{13}C)$ (difference of 0.5 ppm), which is expected to be more sensitive towards differences in packing of the chains than $\delta_{iso}(^{19}F)$ and $\delta_{iso}(^{119}Sn)$ because of the methyl group location on the periphery of the chains. The extremely weak interchain forces result in the fragility

of $(CH_3)_3SnF$ crystals and the observation of a separate room-temperature phase with kinetically controlled chain packing.

Experimental

Trimethyltin fluoride was prepared by metathesis reaction of trimethyltin chloride with potassium fluoride according to the literature.[2]

IR $\nu_{as}(CH_3)$: 2995m, $\nu_s(CH_3)$: 2921m, $\delta(CH_3)$: 1210, 1185m, $\rho(CH_3)$: 773s, $\nu_s(SnC_3)$: 551s cm^{-1}. Raman $\nu_{as}(CH_3)$: 2998(4), $\nu_s(CH_3)$: 2924(15), $\delta_s(CH_3)$: 1208(16), $\nu_{as}(SnC_3)$: 556(29), $\nu_s(SnC_3)$: 520(100), 196(12), $\delta_s(SnC_3)$: 144 (34) cm^{-1}.

NMR Spectroscopy

High-resolution ^1H, ^{19}F, ^{119}Sn, and ^{13}C solid-state MAS NMR spectra were recorded using a 500 MHz Bruker Avance III HD NMR spectrometer equipped with T-3 Varian four-channel HFXY probes, with Larmor frequencies 499.30, 469.75, 186.20, and 125.55 MHz, respectively. The appropriate recycle delay for each nucleus was determined by saturation recovery. The pulse widths were calibrated by nutation measurements. All chemical shifts reported are with respect to $Si(CH_3)_4$ for ^1H and ^{13}C, $Sn(CH_3)_4$ for ^{119}Sn, and $CFCl_3$ for ^{19}F, using adamantane (^1H: 1.63 ppm; ^{13}C: −38.5 ppm), hexafluorobenzene (^{19}F: −166.4 ppm) and SnO_2 (^{119}Sn: −604.3 ppm) as a secondary references. Experimental NMR spectra were simulated using the program SIMPSON.[18] The Mehring convention was used for describing the properties of the shielding tensor, using the isotropic chemical shift δ_{iso}, the chemical shift anisotropy δ_{aniso}, and the asymmetry factor η given by

$$\delta_{iso} = \frac{1}{3}(\delta_{xx} + \delta_{yy} + \delta_{zz})$$

$$\delta_{aniso} = \delta_{zz} - \delta_{iso}$$

$$\eta = \frac{\delta_{xx} - \delta_{yy}}{\delta_{aniso}}$$

with $|\delta_{zz} - \delta_{iso}| \geq |\delta_{xx} - \delta_{iso}| \geq |\delta_{yy} - \delta_{iso}|$

All spectra were recorded using either the 2.5 or 3.2-mm four-channel HFXY probe with maximum spinning rates of 30 or 25 kHz, respectively. The maximum powers used for the 2.5 and 3.2-mm probes were 125 and 100 kHz, respectively. For each nucleus, experiments were performed at two or more spinning frequencies ranging from 12-24 kHz to unambiguously identify the centre band.

High-resolution, simultaneously ^{1}H- and ^{19}F-decoupled ^{13}C NMR spectra were collected using the four-channel 3.2-mm (non-recrystallized)/2.5-mm (recrystallized) probe in three-channel ^{1}H-^{19}F-^{13}C mode. The ^{13}C{^{1}H,^{19}F} NMR spectra were measured using a 90° pulse width of 2.0 µs, a recycle delay of 30 s, and a spinning rate of 21 kHz. A total of 1700/5000 transients were recorded as 2000/4090 complex points over an acquisition time of 20.00/20.45 ms for the non-recrystallized/recrystallized sample. For the non-recrystallized sample, simultaneous CW decoupling was used with powers of 60 and 40 kHz on the ^{1}H and ^{19}F channels, respectively. For the recrystallized sample, CW and XY16 decoupling was used with powers of 71.4 and 125 kHz on the ^{1}H and ^{19}F channels, respectively.

^{1}H{^{19}F} NMR spectra were measured using the Direct-polarization (DP) and Cross-polarization (CP) methods. The DP ^{1}H{^{19}F} NMR spectra were obtained using the 2.5-mm four-channel HFXY probe in three-channel-HFC mode, with a 90° pulse width of 2.0 µs and a recycle delay of 15 s. A total of 16 transients were recorded over an acquisition time of 4.096 ms as 2048 complex points, under ^{19}F-decoupling power of 50 kHz. The ^{19}F- to ^{1}H- CP MAS ^{1}H{^{19}F} NMR spectrum, was obtained under the Hartmann-Hahn matching condition at 40.6 kHz RF power and at an optimum a contact time of 2.5 ms. A total of 136 transients were recorded under the same

conditions as reported for the DP experiment. Likewise, the $^{19}F\{^{1}H\}$ NMR spectra at various spinning rates were collected using the 2.5-mm four-channel HFXY probe, using a 90° pulse width of 3.0 μs and the recycle delay of 360 s. Twenty four to 200 transients were recorded as 5978 complex points over an acquisition time of 14.945 ms, under a ^{1}H-decoupling power of 63 kHz and a spinning rate of 12 to 24 kHz.

The high-resolution simultaneously decoupled $^{119}Sn\{^{1}H,^{19}F\}$ NMR spectra were collected using 2.5-mm four-channel probe in three-channel ^{1}H-^{19}F-^{119}Sn mode using a 90° pulse width of 5.0 μs and a recycle delay of 60 s at spinning rates of 15.5 and 24 kHz. A total of 522/586 transients were collected as 2528/4968 complex points over an acquisition time of 4.045/7.949 ms for non-recrystallized/recrystallized $(CH_3)_3SnF$. Fluorine-19 XY-16 decoupling employed decoupling powers of 100 kHz, while simultaneous ^{1}H decoupling utilized 83 kHz (TPPM15)/62.5 kHz (CW) for non-recrystallized/recrystallized $(CH_3)_3SnF$, resulting in line widths of 350 Hz.

The high-resolution $^{119}Sn\{^{1}H\}$ NMR spectra were collected using the 2.5-mm four-channel HFXY probe in three-channel ^{1}H-^{19}F-^{119}Sn mode at different spinning rates. The pulse width used was 4.0 μs with a recycle delay of 60 s, and an acquisition time of 8.947 ms was used for 5592 complex points. The CW decoupling power on the ^{1}H channel was 62.5 kHz. A total of 1400 or 750 scans was collected giving line widths obtained was of 390 Hz.

Crystallography

Crystals of $(CH_3)_3SnF$ were grown from hot ethanol by allowing the solution to slowly cool from 60 °C to room temperature. Crystals were mounted at low temperature under a stream of dry cold nitrogen as previously described.[19] The crystals were centered on a Bruker SMART APEX II diffractometer, controlled by the APEX2 Graphical User Interface software.[20] The program SADABS[21] was used for the scaling of diffraction data, the application of a decay correction, and

a multi-scan absorption correction. The program SHELXS-97[22] was used for structure solution and SHELXL-2014/6[23] for refinement. Structure solutions were obtained by direct methods. CCDC 1400761 and 1400762 contain the crystallographic data for $(CH_3)_3SnF$ at 23 and −120 °C, respectively. These data can be obtained free of charge from The Cambridge Crystallographic Data Centre via www.ccdc.cam.ac.uk/data_request/cif.

Powder X-Ray Diffraction

(a) Variable-temperature powder X-ray diffraction patterns were obtained on the Bruker SMART APEX II diffractometer used the Kα radiation (λ = 0.71073 Å) of a Mo X-ray source. A melting point capillary was filled with the powder samples and the powder X-ray diffraction pattern was acquired using the XRD[2] evaluation plug-in of the APEX2 Graphical User Interface software.[20]

(b) Powder X-ray patterns were recorded at room temperature in Bragg-Brentano geometry using a PANAlytical X'Pert Pro diffractometer equipped with a Cu-anode ($\lambda(Cu\text{-}K\alpha_1)$ = 1.540598 Å, $\lambda(Cu\text{-}K\alpha_2)$ = 1.544426 Å) using 0.04 rad soller slits, a 1/8° divergence slit, a quartz zero background sample holder, a diffracted beam Ni-filter and an X'Celerator microstrip detector with 128 detector elements. The diffractograms were recorded covering $5° \leq 2\theta \leq 55°$ in 0.0083° steps with 200 s/step counting time. The sample was cast as a thin film from an acetone slurry and was spun at 1 rotation per second. The diffraction data for the crystalline phase were analyzed with the FullProf.2k. program suite[24] using the LeBail method. A total of 20 parameters were refined, including the 3 unit cell axes, 3 peak shape parameters, 2 asymmetry parameters and the background described by 12 linearly interpolated points. Seven angular ranges were excluded from the refinement because of the presence of the phase impurity. The excluded regions are clearly highlighted in Figure 3.

Acknowledgements

We are thankful to the Natural Sciences and Engineering Research Council of Canada (NSERC) (MG, PH, MB), the University of Lethbridge (MG, PH), the Canada Foundation for Innovation (CFI) (MG, PH, MB) and the Manitoba Foundation for Innovation (MFI) (MB) for providing funding for this research. PC is thanking Alberta Innovates - Technology Futures for a Graduate Scholarship and the Len Bolger Scholarship. We would also like to thank Charles Campana for helpful discussions and Tony Montina (manager of the NMR facility at the University of Lethbridge) for help with the NMR experiments. The authors also like to thank the anonymous reviewers whose comments helped to improve this publication.

References:

1. a) A. Herzog, F. Q. Liu, H. W. Roesky, A. Demsar, K. Keller, M. Noltemeyer and F. Pauer, *Organometallics* 1994, **13**, 1251; (b) E. F. Murphy, R. Murugavel and H. W. Roesky, *Chem. Rev.*, 1997, **97**, 3425.
2. E. Krause, *Ber. Dtsch. Chem. Ges*. 1918, **51**, 1447.
3. H. C. Clark, R. J. O'Brien and J. Trotter, *J. Chem. Soc*. 1964, 2332.
4. K. Yasuda, Y. Kawasaki, N. Kasai and T. Tanaka, *Bull. Chem. Soc. Jpn.* 1965, **38**, 1216.
5. H. Reuter and H. Puff, *J. Organomet. Chem.* 1989, **379**, 223.
6. S. Al-Juaid, S. M. Dhaher, C. Eaborn, P. B. Hitchcok, J. D. Smith, *J. Organomet. Chem.*, 1987, **325**, 117.
7. D. Tudela, E. Gutiérrez-Puebla and A. Monge, *J. Chem. Soc., Dalton Trans.*, 1992, 1069.
8. H. Reuter, Ph.D. Thesis, University of Bonn, 1986.
9. J. Beckmann, D. Horn, K. Jurkschat, F. Rosche, M. Schürmann, W. Zachwieja, D. Dakternieks, A. Duthie and A. E. K. Lim, *Eur. J. Inorg. Chem.*, 2003, 164.
10. D. Tudela, R. Fernandez, V. K. Belsky and V. E. Zavodnik, *J. Chem. Soc., Dalton Trans.*, 1996, 2123.
11. S. Calogero, P. Ganis, V. Peruzzo, G. Tagliavini and G. Valle, *J. Organomet. Chem.* 1981, 220, 11.
12. L. N. Zahkarov, Yu. T. Struchkov, E. A. Kuz'min and B. I. Petrov, *Kristallografiya*, 1983, **28**, 271.
13. H. Bai, R. K. Harris and H. Reuter, *J. Organomet. Chem.*, 1991, **408**, 167.
14. J. C. Cherryman and R. K. Harris, *J. Magn. Res.*, 1997, **128**, 21.
15. H. Bai and R. K. Harris, *J. Magn. Reson*., 1992, **96,** 24.

16. T. P. Lockhart and W. F. Manders, *J. Am. Chem. Soc.*, 1985, **107**, 5863.

17. T. P. Lockhart and W. F. Manders, *J. Am. Chem. Soc.*, 1987, **109**, 7015.

18. M. Bak, J. T. Rasmussen, N. C. Nielsen, *J. Magn. Reson.*, 2000, **147**, 296.

19. M. Gerken, D. A. Dixon, G. J. Schrobilgen, *Inorg. Chem.*, 2000, **39**, 4244-4255.

20. APEX 2; Bruker AXS Inc.; Madison, WI, 2006.

21. G. M. Sheldrick, *SADABS*, Version 2007/4, Bruker ACS Inc.; Madison, WI, 2007.

22. G. M. Sheldrick, SHELXTL97, University of Göttingen, Germany, 2008.

23. G. M. Sheldrick, SHELXTL-2014, University of Göttingen, Germany, 2014.

24. J. Rodriguez-Carvajal, *Full Prof.2k, Version 5.40; 2014. http://www.ill.eu/sites/fullprof/.*